



The High Enthalpy Shock Tunnel Göttingen of the German Aerospace Center (DLR)

Institute of Aerodynamics and Flow Technology
Bunsenstraße 10
37073 Göttingen *

Scientists:

- Dr. Jan Martinez Schramm, Jan.Martinez@dlr.de
- Dr. Alexander Wagner, Alexander.Wagner@dlr.de
- Dr. Divek Surujhlal, Divek.Surujhlal@dlr.de
- Dr. Giannino Ponchio Camillo, Giannino.PonchioCamillo@dlr.de

Abstract: The High Enthalpy Shock Tunnel Göttingen (HEG) of the German Aerospace Center (DLR) is one of the major European hypersonic test facilities. It was commissioned for use in 1991 and was utilized since then extensively in a large number of national and international space and hypersonic flight projects. Originally, the facility was designed for the investigation of the influence of high temperature effects such as chemical and thermal relaxation on the aerothermodynamics of entry or re-entry space vehicles. Over the last years its range of operating conditions was subsequently extended. In this framework the main emphasis was to generate test conditions which allow investigating the flow past hypersonic flight configurations from low altitude Mach 6 up to Mach 10 in a wide altitude range. The studies performed in HEG focused on external as well as internal aerodynamics including combustion of hydrogen in supersonic combustion, shock-wave boundary layer interaction, the investigation and control of boundary layer transition in hypersonic flows and hypersonic turbulence.

1 Introduction

In hypervelocity flows the speed of the considered fluid is much larger than the speed of sound. Commonly the hypersonic flow regime is considered to start above a Mach number of $M=5$. Ground based testing of such flows is performed in a large variety of facilities. The reason for this is the enormous range of flow conditions and phenomena encountered in hypersonic flight and the fact that no single facility can simulate all relevant flow parameters simultaneously. Therefore, in hypersonic testing,

*Cite article as: Deutsches Zentrum für Luft- und Raumfahrt (DLR). (2024). The High Enthalpy Shock Tunnel Göttingen of the German Aerospace Center (DLR). *Journal of large-scale research facilities*, 9, A188. <http://dx.doi.org/10.17815/jlsrf-9-188>



partial simulation of different flow phenomena is performed in different types of facilities. Examples are Mach-Reynolds number simulation in cold hypersonic ground based test facilities, verification and qualification of hot structures of space vehicles in arc-heated test facilities or the investigation of the influence of chemically reacting flow past an entry or re-entry vehicle on its aerodynamic behavior in shock tunnels or shock expansion tunnels. Comprehensive overviews of ground based testing of hypersonic flows are given by e.g. Lu & Marren (2002) or Lukasiewicz (1973).

One possibility to increase the Mach number in ground based facilities is to reduce the free stream temperature, i.e. the free stream speed of sound. Here, correct similarity Mach numbers can be achieved, even though the free stream velocity is significantly lower than the actual flight velocity. However, characteristic of high Mach number hypersonic flight with $M \approx 10$ and above is that the kinetic energy of the flow is high enough to effectuate high temperature effects such as vibrational excitation or dissociation of the fluid molecules in the flow past hypersonic vehicles. The high flow velocities and subsequently the high temperature effects are not duplicated in cold hypersonic test facilities.

During the re-entry flight of a space vehicle in the earth's atmosphere or the interplanetary atmospheric entry of space vehicles or meteorites, speeds in excess of 6 km/s are achieved. To establish a flow with this speed in a test section with an area of 1 m^2 and a density of 3 g/m^3 , a power requirement of already 300 MW is needed. Therefore, continuous flow facilities are not a practical way to generate such high enthalpy, hypersonic flows. Additionally, the correct simulation in ground based testing of the chemical relaxation length of the dissociation reactions of the fluid molecules occurring for example behind the strong bow shock in front of the nose of a re-entry vehicle, requires the duplication of the flight binary scaling parameter ρL ; the product of the free stream density ρ and a characteristic flow length L . Consequently, the smaller the scale of the wind tunnel model is chosen, the higher the free stream density or pressure needs to be. Considering the flight trajectory range of a re-entry vehicle in about 70 km altitude, where typically the highest heat flux into the structure occurs, the atmospheric density is approximately 0.1 g/m^3 . Using a geometrical scaling factor of 30, a free stream density in the ground based facility of 3 g/m^3 is required.

If a flow with the above free stream density and a velocity of 6 km/s is generated by expansion in a convergent - divergent hypersonic nozzle from a reservoir at rest without adding energy, a total specific enthalpy of about 23 MJ/kg and a nozzle reservoir pressure in the order of 90 MPa is required. This results in a nozzle reservoir temperature of about 10000 K. At reasonable costs, such conditions can only be achieved in impulse facilities with short flow duration.

The most successful facility types which are able to generate high enthalpy and high pressure hypersonic flows are shock tunnels and shock expansion tunnels with typical test times of approximately 5 milliseconds and less. The principle of these facilities is to store the energy over a long period of time, therefore reducing the necessary power requirement and subsequently releasing the stored energy rapidly. Due to the high flow speeds, test times in the order of a few milliseconds are still sufficient for the development of a steady flow over a model. A reasonable, conservative correlation of the necessary test time to establish a steady flow is $\tau = 20 L/u_\infty$, where L is the model length and u_∞ is the free stream velocity. For a test using the above mentioned flow condition and a 0.3 m long wind tunnel model, the required test time would be 1 ms.

The high pressure, high velocity flows which can be generated in shock tunnels and shock expansion tunnels makes these facilities not only suitable for the investigation of space vehicle aerothermodynamics but also for studying complete air breathing propulsion systems, particularly supersonic combustion ramjets (scramjets) at flight Mach numbers of $M = 8$ and above. In this framework it is important that in addition to the free stream Mach and Reynolds number, the correct static pressure and temperature are established in the combustor. Further, if hypersonic flight configurations are considered which can be tested at 1:1 scale, the flight free stream conditions can be duplicated in these facilities generating the same pressure and heat flux loads as experienced in flight. In the subsequent sections, the operating conditions realized in HEG will be presented.

2 High Enthalpy Shock Tunnel Göttingen (HEG)

The HEG is a free piston driven shock tunnel and was developed and constructed in the framework of the European HERMES program over the period 1989 – 1991. It was commissioned for use in 1991, at that time being the largest facility of its type worldwide. Since then it was extensively used in a large number of national and international space and hypersonic flight projects. The research activities are always strongly linked to computational fluid dynamics (CFD) and comprise for instance the calibration process of the facility (Hannemann, 2003), the study of generic aerodynamic configurations including the investigation of fundamental aspects of high enthalpy flows (G. Camillo & Wagner, 2023; Karl et al., 2005; Surujhlal et al., 2022; Wagner, Martinez Schramm, et al., 2016), complex hypersonic flight configurations (Ecker et al., 2023; Karl & Steelant, 2018; Wagner et al., 2019), integrated scramjet configurations (Martinez Schramm et al., 2008; Schramm & Luís, 2021; Schramm & Schmidt, 2021) and hypersonic boundary layer transition and transition control strategies (Laurence et al., 2014; Sandham et al., 2014; Surujhlal et al., 2023; Wagner et al., 2013).

In a free piston driven shock tunnel, the conventional driver of a shock tunnel is replaced by a free piston driver. This concept was proposed by Stalker (1967). A schematic and a (x,t) wave diagram of this facility type is shown in Figure 1. Free piston driven shock tunnels consist of an air reservoir behind the piston, a compression tube, separated from an adjoining shock tube via the primary diaphragm, and a subsequent nozzle, test section and dump tank.

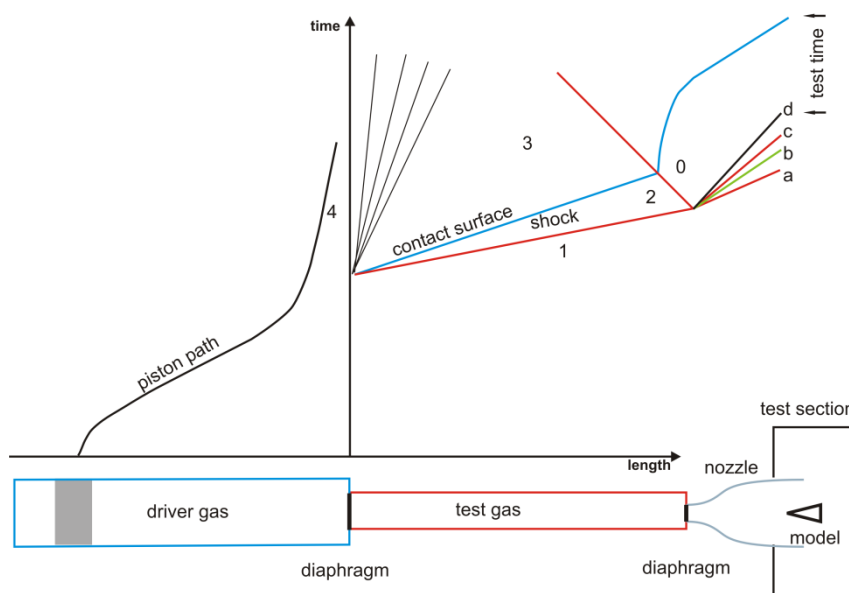


Figure 1: Schematic of a free piston driven shock tunnel and the wave (x-t) diagram.

A schematic of HEG is given in Figure 2. The high pressure air stored in the secondary reservoir is utilized to accelerate a heavy piston down the compression tube. During this quasi-adiabatic compression and heating of the light driver gas (typically helium or a helium argon mixture) the piston reaches a maximum velocity in the order of 300 m/s. The driver gas temperature increases with the driver gas volumetric compression ratio. When the main diaphragm burst pressure is reached it ruptures and the wave process as in a conventional reflected shock tunnel is initiated (see Figure 1). A shock wave is moving into the driven section and the head of a centered expansion wave is moving into the high pressure region. The numbers used in Figure 1 denote distinct regions of the flow. Region 1 contains the test gas at the initial shock tube filling conditions and region 4 contains the hot, compressed driver gas after piston compression. Region 2 contains the shock compressed test gas, while in region 3, the driver gas processed by the unsteady expansion wave is contained. The test and driver gas are separated by a contact surface.

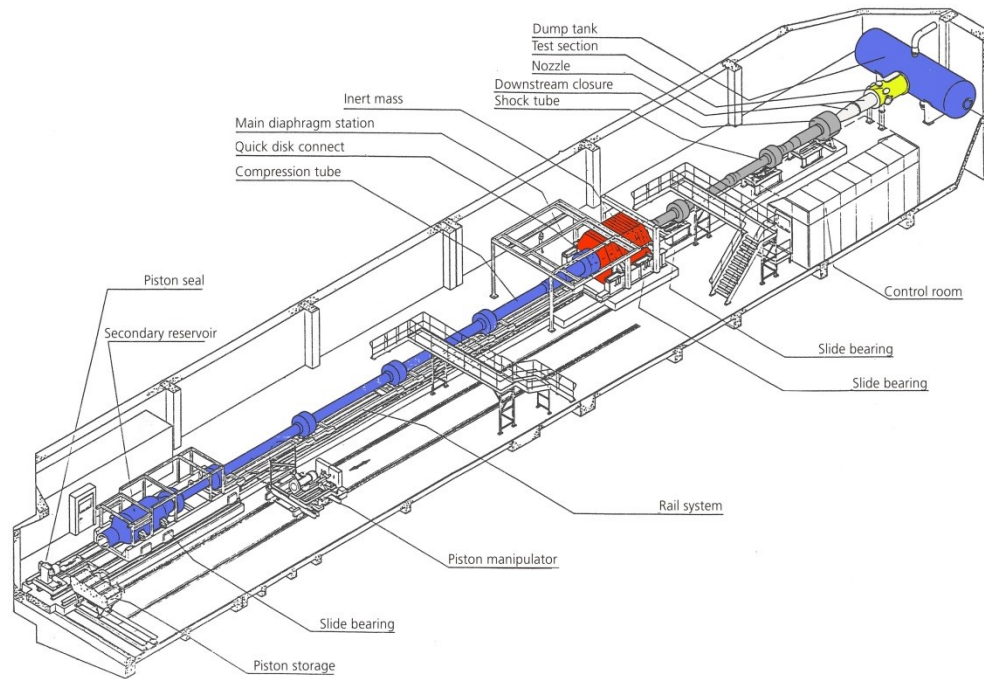


Figure 2: Schematic of the High Enthalpy Shock Tunnel Göttingen, HEG.

After reflection of the incident shock wave at the right end wall of the shock tube, the test gas is brought to rest in region 0. Subsequently, the reflected shock wave penetrates the contact surface. Depending on the local conditions, three types of shock wave / contact surface interaction are obtained, namely tailored, undertailored, or overtailored. Due to the fact that the shock-compressed and heated slug of gas in region 0 is used in reflected shock tunnel operation as the reservoir driving the flow in the nozzle and test section, shock tube operation in tailored interface mode is most desirable. At this condition the pressure in region 0 remains constant. For undertailored or overtailored interface conditions, the pressure in region 0 is decreasing or increasing, respectively, after interaction of the reflected shock with the contact surface.

Reflected shock tunnels are characterized by a convergent - divergent nozzle which is attached to the end of the shock tube. A thin secondary diaphragm is placed at the nozzle entrance in order to allow evacuation of the nozzle, test section and vacuum tank before the run. The nozzle entrance diameter is chosen sufficiently small such that the incident shock wave is almost completely reflected. The stagnant slug of test gas, generated by the shock reflection in region 0, is subsequently expanded through the hypersonic nozzle.

The nozzle flow starting process is characterized by a wave system which passes through the nozzle before a steady flow is established (see Figure 1). The incident shock wave (a) is followed by a contact surface (b), an upstream facing secondary shock wave (c) and the upstream head of an unsteady expansion (d). The trajectory of the piston is chosen in a way that after main diaphragm rupture, the pressure and temperature of the driver gas in region 4 is maintained approximately constant. This is achieved by selecting the velocity of the piston at diaphragm rupture, and therefore the subsequent movement of the piston such that it compensates for the loss of the driver gas flowing into the shock tube. For that reason, in contrast to the constant volume driver of conventional shock tunnels, the free piston driver is a constant pressure driver. Due to the large forces occurring during the operation of the free piston driver, the compression tube, shock tube, nozzle assembly is allowed to move freely in axial direction. An inert mass placed at the compression tube / shock tube junction significantly reduces the recoil motion of the facility during operation. The test section and the vacuum tank remain stationary.

A sliding seal is used at the nozzle / test section interface.

The overall length of HEG is 62 m and it weighs approximately 280 t. A third of its weight is contributed by an inert mass (see Figure 1 and left picture of Figure 3) which is used to reduce the tunnel recoil motion. The compression tube is closed by a hydraulic oil system (quick disk connect) at the main diaphragm station. The shock tube is connected to the nozzle of the tunnel at the downstream closure, which is also driven by oil hydraulics to close and seal the tunnel. The compression tube has a length of 33 m and a diameter of 0.55 m. The shock tube is 17 m long with a diameter of 0.15 m. The HEG was designed to provide a pulse of gas to a hypersonic convergent - divergent nozzle at stagnation pressures of up to 200 MPa and stagnation enthalpies of up to 23 MJ/kg. Regarding the test gas, no basic limitations exist. The operating conditions presented in the present article are related to the test gas air. Additionally, operating conditions using nitrogen and carbon dioxide exist.

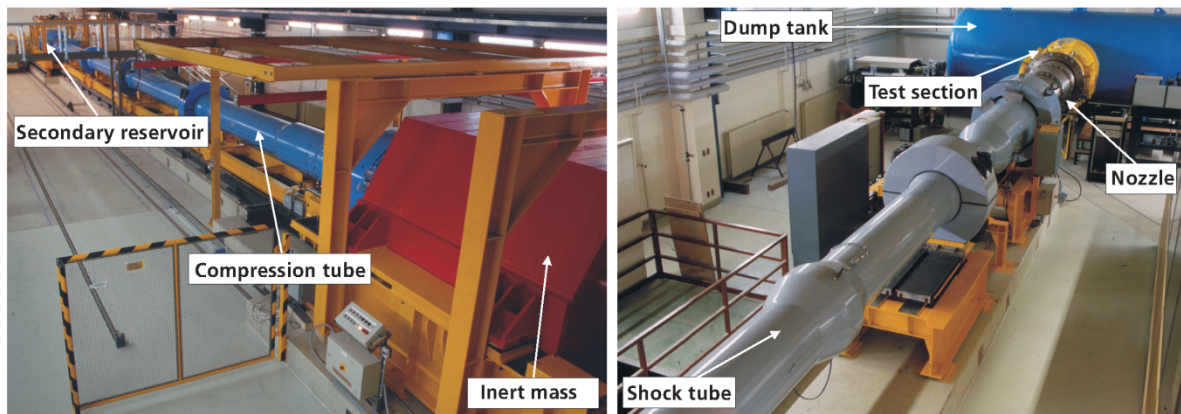


Figure 3: Photographic views of the High Enthalpy Shock Tunnel Göttingen, HEG.

3 HEG Operating Conditions

Originally, HEG was designed for the investigation of the influence of high temperature effects such as chemical and thermal relaxation on the aerothermodynamics of entry or re-entry space vehicles. As discussed above, in order to correctly model the chemical relaxation occurring behind the bow shock of a re-entry vehicle the flight binary scaling parameter ρL must be reproduced in ground based testing. Further, for high enthalpy testing an additional driving parameter which must be reproduced is the flow velocity. Therefore, a selection of operating conditions of HEG are presented in Figure 4 in terms of the binary scaling parameter ρL and the flow velocity u . Here L represents the length of the considered configurations.

In addition to the HEG operating conditions (represented by the filled circles), the most important fluid mechanical and chemical processes occurring during re-entry of a spacecraft in the Earth's atmosphere are depicted in Figure 4. Further, as a reference the flight trajectories of a lifting body re-entry from low Earth orbit (IXV), a ballistic superorbital re-entry (Apollo 11) and a hypersonic flight experiment (SHEFEX) are provided. An indication of the corresponding flight altitudes is given in the right diagram of Figure 4 showing the temperature variation of the Earth's atmosphere. The transitions between regimes of different physical and chemical properties shown in Figure 4 depend on the chosen reference length and vary when different configurations are considered. Further, the boundaries shown have only symbolic character. In reality, no clear-cut dividing lines between the different regimes exist. The Knudsen number given in Figure 4 shows that the HEG operating conditions are located in the continuum flow regime. The high energy content of re-entry flows leads to strong heating of the air in the vicinity of a spacecraft. Depending on the temperature level behind the shock wave (i.e. the flight velocity), the vibrational degrees of freedom of the air molecules are excited and dissociation reactions of oxygen- and nitrogen molecules may occur. Further, ionization of the air constituents occurs. The

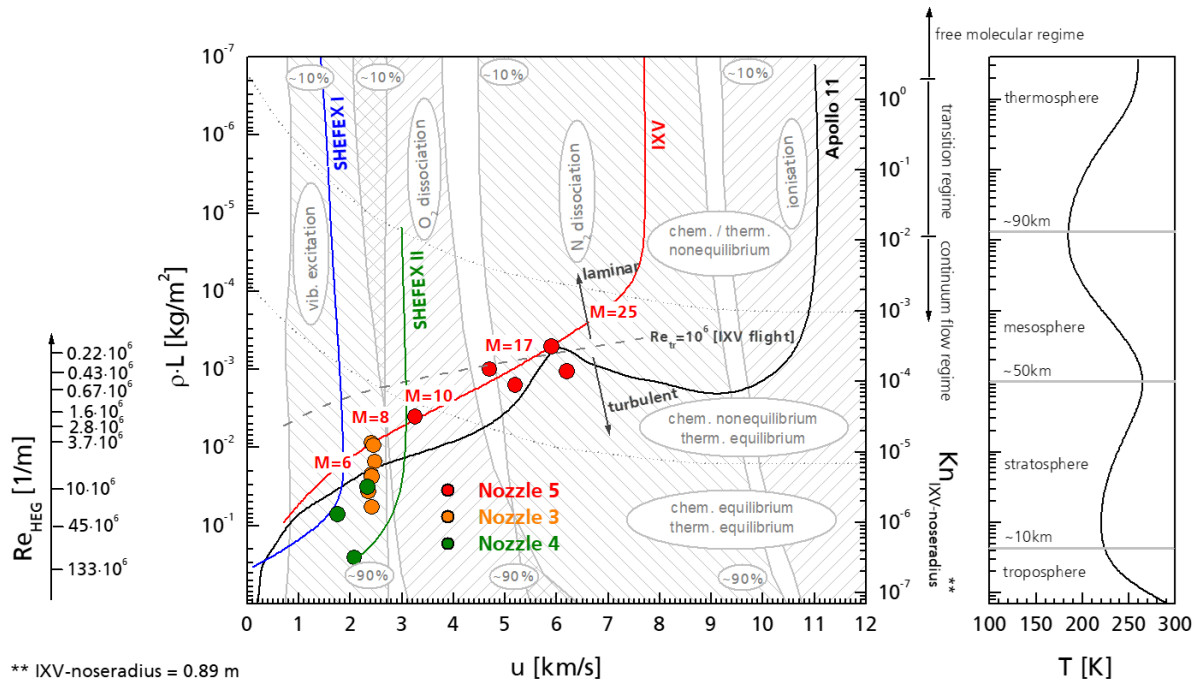


Figure 4: HEG operating range in terms of the binary scaling parameter ρL and the flow velocity u .

high temperature effects described here are enabled by energy transfer from the translational energy stored in the random motion of the air particles, which is increased by the gas heating, to other forms of energy. Because this energy transfer is realized by air particle collisions, it requires a certain time period to develop. The time required to reach an equilibrium condition, is e.g. defined by the local temperature and density. Therefore, depending on the ratio of the relaxation time to a characteristic timescale of the flow, the chemical and thermal relaxation processes can be either in non-equilibrium or in equilibrium.

Further, along a re-entry trajectory, the Reynolds number varies over several orders of magnitude. In high altitude flight the wall boundary layer of a re-entry vehicle is initially laminar. After exceeding a critical Reynolds number (shown exemplarily for the IXV configuration in Figure 4 as a black dashed line), the transition from a laminar to a turbulent boundary layer takes place. This process is linked to an increase of the skin friction and the wall heat flux. The HEG operating conditions, depicted with nozzle 5 in Figure 4, are the original high enthalpy conditions covering a total specific enthalpy range from 12 – 23 MJ/kg. These conditions have been used for the investigation of several re-entry configurations including ARD, X-38, EXPERT, ExoMars or Pre-X / IXV.

Over the last years the HEG operating range was subsequently extended. In this framework the main emphasis was to generate test conditions which allow investigating the flow past hypersonic flight configuration from low altitude Mach 6 up to Mach 10 in a large altitude range. These low enthalpy conditions cover the range of total specific enthalpies from 1.5 – 6 MJ/kg. For 1:1 scale wind tunnel models, the conditions with nozzle 3 depicted in Figure 4 duplicate $M = 7.4$ flight conditions in 28 km and 33 km, respectively. They were used for instance for the ground based testing of the HyShot II and IV supersonic combustion flight experiment configurations as described in Martinez Schramm et al. (2008) and Karl et al. (2008).

Additional conditions, depicted with nozzle 4 in Figure 4, duplicate $M = 6$ flight conditions between sea level and 15 km altitude. These conditions were used in the framework of the SHEFEX I post flight analysis and the investigation of the intake of the LAPCAT (EC project Long-Term Advanced Propulsion Concepts and Technologies) $M = 8$ aircraft (Martinez Schramm et al., 2009). The $M = 10$ condition duplicates flight conditions at 33 km altitude, and has been used in the framework of the

DLR SHEFEX II project and for the ground-based testing of a scramjet flight experiment configuration (Boehrke et al., 2012).

In Figure 5, the low enthalpy HEG operating conditions are given in terms of Mach and Reynolds number. The Reynolds number is based on the length of the considered configurations. As reference, the trajectories of the flight configurations SHEFEX I and II, HyShot II and IXV are provided.

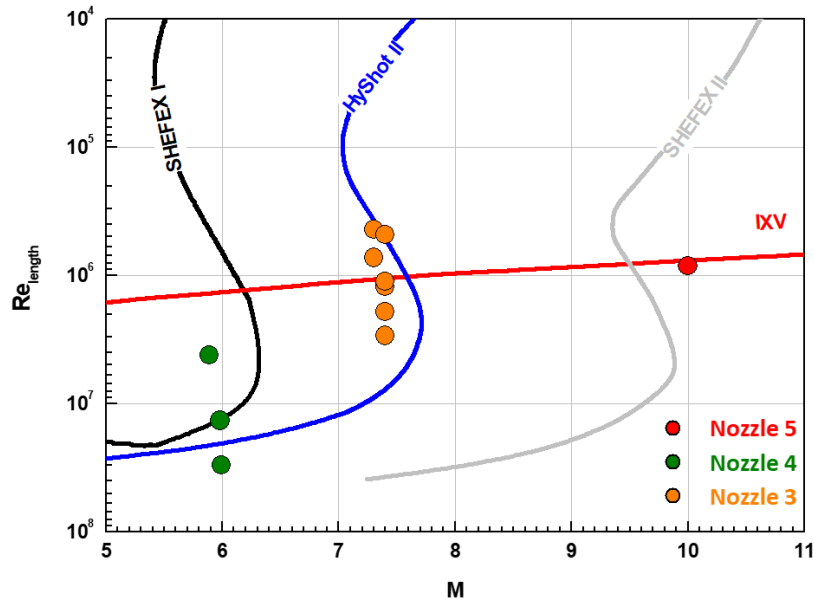


Figure 5: HEG operating conditions in terms of Mach and Reynolds number.

Details of the HEG operating conditions discussed above are provided in Table 1, 2, and 3. In the reservoir nomenclature in the tables, H is used to denote the total enthalpy and R the unit Reynolds number. In order to realize the operating conditions, a series of different Laval nozzles had to be designed, constructed and implemented in HEG. The nozzle which is used to expand the test gas to the targeted free stream is given in the header of each table. The test time for the high enthalpy conditions is in the range of 1 ms. For the low enthalpy conditions, the test time ranges from 3 to 8 ms. The nozzles used to generate the corresponding test conditions are illustrated in Figure 6. Details of the operational HEG nozzles are provided in the following section. Further, different pistons are utilized on HEG for generating different operating conditions. In order to allow a large flexibility in tuning new operating conditions, four pistons (without brakes) with different weight (275 kg, 481 kg, 700 kg and 815 kg) are available. An additional 848 kg piston with brakes can be utilized.

4 Set of HEG Nozzles

The nominal nozzle design Mach numbers, area ratios and lengths are given in Figure 6. Please note that for the high enthalpy conditions the Mach number is lower than the corresponding flight Mach number (see also Figure 4) due to chemical and thermal freezing effects during the nozzle expansion. However, for high enthalpy testing the Mach number is of less importance and the flight velocity must be reproduced correctly.

Due to the different nozzle length, a second test section was built for nozzle 3. When utilizing nozzle 4, an additional adapter ring is used between the second and the main test section. The nozzle – test section assembly using the three HEG nozzles is shown in Figure 7. Depending on the chosen operating condition and the angle of attack, model configurations with a typical length between 0.4 m and 1.0 m and a width of up to 0.4 m can be mounted in the test sections. In case the major emphasis of the tunnel testing is on the investigation of internal flow paths (e.g., scramjet combustors), models of up to 2.0 m

Nozzle	3								
Reservoir	H3.3R1.5	H3.4R1.6	H3.5R2.4	H3.3R3.7	H3.2R4.1	H3.0R6.4	H3.4R9.8	H11.9R1.5	H9.8R2.2
p_0 [MPa]	6.8	8.0	12.7	17.0	19.2	28.4	47.3	37.6	44.1
T_0 [K]	2720	2810	2895	2740	2734	2582	2835	6816	5932
h_0 [MJ/kg]	3.3	3.4	3.5	3.3	3.2	3.0	3.4	11.9	9.8
M_∞ [-]	7.3	7.4	7.3	7.4	7.4	7.4	7.4	6.1	6.2
Alt (p_∞) [km]	33	32	29	27	26	24	20	19	18
Alt (ρ_∞) [km]	34	33	30	28	27	24	22	30	28
Re_m [$1/m \cdot 10^6$]	1.5	1.6	2.4	3.7	4.1	6.4	9.8	1.5	2.2
p_∞ [Pa]	789	880	1453	1990	2129	3083	5174	6761	7460
T_∞ [K]	267	277	285	266	268	248	265	1333	1084
ρ_∞ [g/m^3]	10.2	11.0	17.7	25.9	27.6	43.2	67.8	16.9	23.5
u_∞ [m/s]	2409	2450	2480	2410	2422	2350	2419	4426	4036
$Y_{N_2} _{\text{Nozzle exit}}$	-	-	0.7520	-	-	-	-	0.7419	0.7398
$Y_{O_2} _{\text{Nozzle exit}}$	-	-	0.2157	-	-	-	-	0.1639	0.1852
$Y_{NO} _{\text{Nozzle exit}}$	-	-	0.0321	-	-	-	-	0.0539	0.0583
$Y_N _{\text{Nozzle exit}}$	-	-	0.0000	-	-	-	-	0.0000	0.0000
$Y_O _{\text{Nozzle exit}}$	-	-	0.0002	-	-	-	-	0.0404	0.0167

Table 1: Operating conditions using nozzle 3. Species mass fractions at nozzle exit for select conditions are denoted with Y_i . Density and pressure-based altitudes estimation according to the 1976 Standard Atmosphere.

Nozzle	4				
Reservoir	H3.2R14	H2.0R35	H1.5R45	H2.5R101	H2.6R133
p_0 [MPa]	30	32	37	161	188
T_0 [K]	2690	1800	1640	2120	2220
h_0 [MJ/kg]	3.2	2.0	1.5	2.5	2.6
M_∞ [-]	5.7	6.0	6.0	5.8	6.0
Alt (p_∞) [km]	12.7	12.2	11.8	1.4	0.3
Re_m [$1/m \cdot 10^6$]	14	35	45	101	133
p_∞ [Pa]	17540	18815	20100	86249	97800
T_∞ [K]	422	208	221	306	292
ρ_∞ [g/m^3]	144	315	327	977	1160
u_∞ [m/s]	2336	1744	1750	2066	2077

Table 2: Operating conditions using nozzle 4. Pressure-based altitude estimation according to the 1976 Standard Atmosphere.

Nozzle	5				
Reservoir	H6R2.0	H21R0.2	H13R0.5	H23R0.5	H15R0.8
p_0 [MPa]	70	35	44.2	85	90
T_0 [K]	4400	9100	7167	9900	8100
h_0 [MJ/kg]	6.1	21.8	13.0	23.7	15.2
M_∞ [-]	9.2	8.1	8.1	7.7	7.8
Alt (ρ_∞) [km]	30	33	31	26	26
Alt (p_∞) [km]	33	45	40	39	36
Re_m [$1/m \cdot 10^6$]	2.0	0.26	0.5	0.5	0.79
p_∞ [Pa]	1160	793	978	2073	2081
T_∞ [K]	332	1150	824	1449	1042
ρ_∞ [g/m^3]	12.1	2.0	3.9	4.3	6.6
u_∞ [m/s]	3347	5911	4703	6221	5095
$Y_{N_2} _{\text{Nozzle exit}}$	0.7389	0.7554	0.7410	0.75275	0.7420
$Y_{O_2} _{\text{Nozzle exit}}$	0.1997	0.0294	0.1466	0.04867	0.1469
$Y_{NO} _{\text{Nozzle exit}}$	0.0602	0.0249	0.0556	0.03053	0.0536
$Y_N _{\text{Nozzle exit}}$	0.0000	0.0000	0.0000	0.00000	0.0000
$Y_O _{\text{Nozzle exit}}$	0.0012	0.1904	0.0568	0.16805	0.0575

Table 3: Operating conditions using nozzle 5. Species mass fractions at nozzle exit are denoted with Y_i . Density and pressure-based altitudes estimation according to the 1976 Standard Atmosphere.

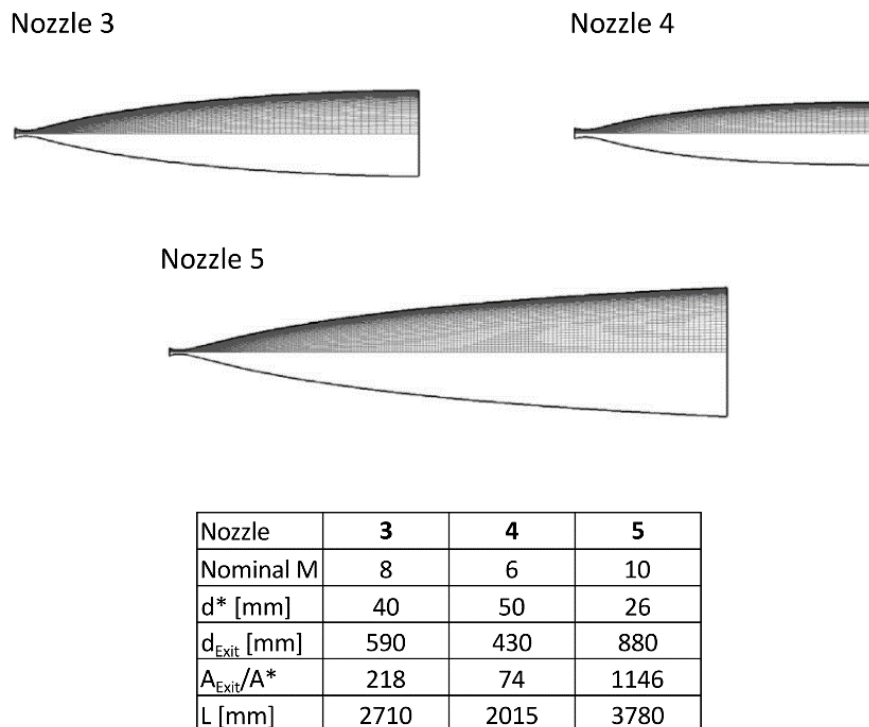


Figure 6: HEG operating conditions in terms of Mach and Reynolds number.

length can be used. The weight of the models is typically less than 200 kg.

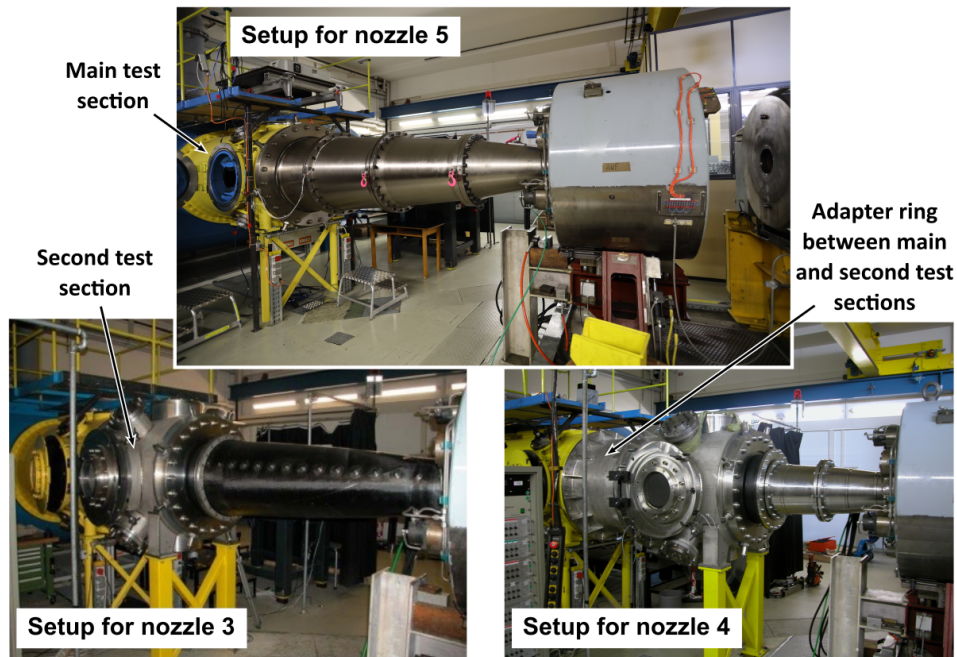


Figure 7: HEG nozzle – test section assembly.

5 HEG Infrastructure

The data acquisition system of HEG consists of a total of 200 channels. Data can be sampled with up to 100 MHz per channel with 16 Bit resolution (SATURN System, AMOtronics GmbH). A gaseous hydrogen injection system has been installed at HEG in order to allow the delivery of hydrogen fuel to wind tunnel models for the investigation of scramjet combustion. The fuel system consists of a 12 mm diameter and 38.4 m long Ludwig tube, and a fast acting solenoid valve. The maximum filling pressure of the Ludwig tube is 15 MPa and it can deliver a pulse of fuel with constant pressure for up to 50 ms. A modular cross arm calibration rake is used for the detailed calibration of the free stream conditions, using Pitot pressure, static pressure and stagnation point heat transfer gauges (see Figure 8).

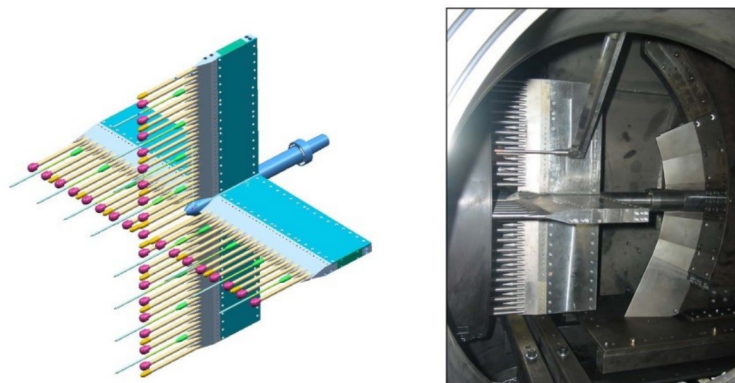


Figure 8: HEG calibration rake – design drawing (left) and rake installed in the test section (right).

6 Calibration Procedure of HEG Operating Conditions

The calibration process of new operating conditions requires a close cooperation between calibration measurements and CFD. This process is discussed here for the HEG condition H3.3R3.7. The numerical determination of the HEG free stream consists of two steps which require a suitable set of input parameters. First, the nozzle reservoir temperature is computed with a one-dimensional analysis of the shock tube. The relevant input parameters are the measured values of the initial shock tube filling pressure and temperature, the shock speed and the nozzle reservoir pressure. Based on these nozzle reservoir conditions, the free stream is subsequently determined by numerical simulation of the nozzle flow using the DLR TAU code. Different RANS turbulence models were applied along with thermal equilibrium and non-equilibrium computations to determine the influence of different modelling assumptions on the computed free stream conditions. It should be noted that for condition H3.3R3.7, the chemical relaxation process is in equilibrium and no free stream dissociation exists. The computational grid consisting of about 20,000 grid points and the Mach number contours resulting from the thermal non-equilibrium computation are shown in Figure 9.

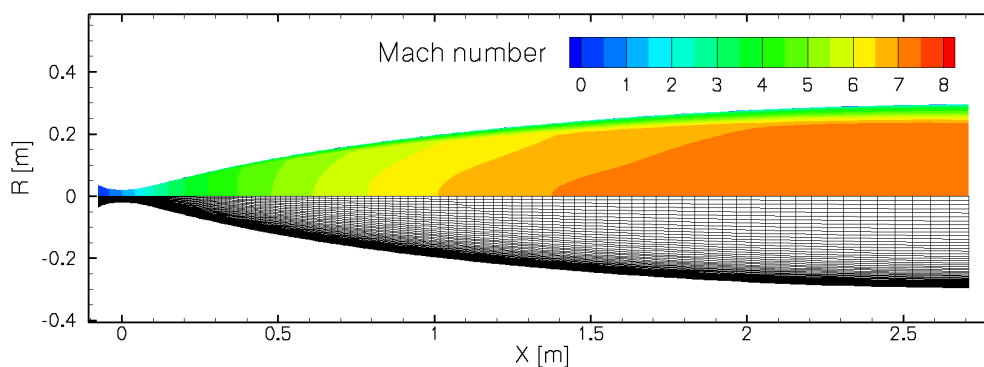


Figure 9: CFD grid and Mach number contours for the HEG nozzle flow (condition H3.3R3.7).

A reservoir-pressure inflow boundary condition is used at the subsonic inflow of the nozzle. The thermodynamic conditions at the inflow are computed using isentropic expansion from prescribed nozzle stagnation conditions using the inflow velocity vector which is part of the CFD solution. The nozzle supply conditions for the considered HEG operating condition H3.3R3.7 is given in Table 1. The chemical non-equilibrium 5 species and 17 reaction rates set for air proposed by Gupta was applied, see Karl et al. (2008). The considered species are molecular and atomic nitrogen and oxygen (N_2 , O_2 , N , O) and nitric oxide (NO). The CFD results are subsequently compared with Pitot pressure and stagnation heat flux measurements on spherical probes and static pressure measurements obtained with the HEG calibration rake.

In Figure 10, the comparison of the measured and computed Pitot pressure, static pressure and stagnation point heat transfer profiles at the nozzle exit plane are shown for HEG condition H3.3R3.7. Regarding the Pitot pressure, the computed data resulting from calculations assuming a thermal equilibrium or thermal non-equilibrium nozzle expansion lie within the experimental scatter bars. The wall boundary layer is assumed to be fully turbulent and the difference due to the application of different turbulence models is negligible. The best agreement between computed and measured Pitot pressure profiles is obtained with the thermal equilibrium assumption and the Wilcox $k-\omega$ turbulence model. The computed static pressure profiles reveal pronounced deviations resulting from the application of different thermal relaxation models. Based on these results it was concluded that the nozzle expansion is in thermal equilibrium. Again, excellent agreement of the numerical and experimental results was achieved using the Wilcox $k-\omega$ turbulence model and the thermal equilibrium assumption. This result shows the importance of performing static pressure measurements even at total specific enthalpy

conditions of approximately 3 MJ/kg. The right plot of Figure 10 shows the comparison of the numerical and experimental normalized stagnation point heat flux profiles. Good agreement with the rake measurements are obtained, however, similar to the Pitot pressure, the stagnation point heat flux measurements are not sensitive to the modelling of the thermal relaxation in the nozzle flow.

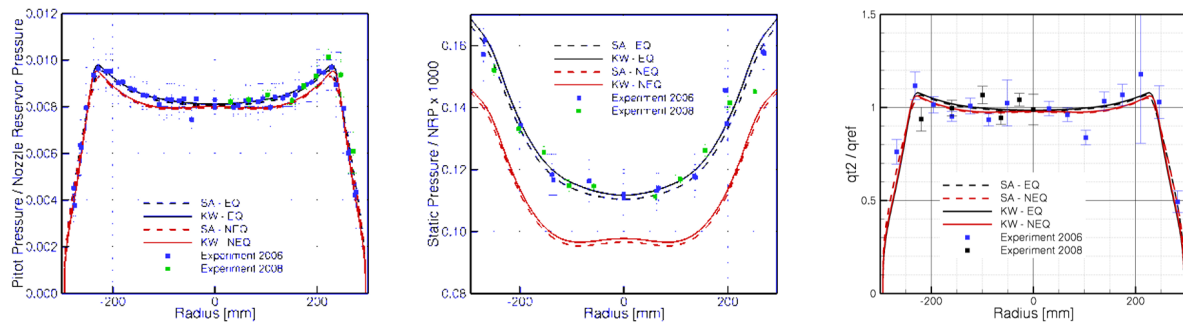


Figure 10: Comparison of measured and computed normalized Pitot pressure (left), static pressure (middle) and stagnation point heat flux distributions at the nozzle exit plane; NEQ: thermal non-equilibrium, EQ: thermal equilibrium, SA: Spalart-Allmaras turbulence model, KW: Wilcox $k-\omega$ turbulence model, NRP: Nozzle reservoir pressure (HEG operating condition H3.3R3.7).

7 Measurement Techniques Overview

The well-established measurement techniques at HEG comprising of surface pressure and heat flux measurements, phase step holographic interferometry and the high speed flow visualisation system (Schlieren / Shadowgraph) are described e.g. in Tropea et al. (2016). Free-stream disturbances can be measured using the probe described in Wagner et al. (2018).

The high speed flow visualization system can be used in conjunction with a digital high speed camera for instance a Shimadzu HPV-1, a Phantom V1210, a Phantom V2012 or a Photron FASTCAM SA-Z type 2100K. The Shimadzu HPV-1 camera is able to record up to 100 frames at a maximum imaging rate of 1 MHz with a resolution of 312x260, while the Phantom V2012 offers a resolution of maximal 1280x800 pixels with an imaging rate of 22.5 kHz. The Photron FASTCAM SA-Z allows a resolution of 1024x1024 pixels at a sampling rate of 20 kHz. The resolution of the latter two cameras can be reduced to achieve significantly higher imaging rates of up to 2.1 MHz. The shuttering of the images is usually achieved by the pulsed laser sources and can be adjusted down to 10 ns for high frequencies (Cavitar Cavilux HF systems).

An internal multiple component stress wave force balance was designed, calibrated and tested in HEG (Robinson & Hannemann, 2006). The balance is able to measure forces (approximately 50 to 5000 N) within 1 - 5 ms on instrumented models at angles of attack from -40° to 20° . The accuracy of the force balance is estimated at approximately $\pm 5\%$ for the axial component and $\pm 4\%$ for the normal and pitching moment components. Additional force measurement techniques based on external stress wave force balances, accelerometer based and free flight based force measurement techniques have been developed and implemented in the past years, Friedl et al. (2016); Laurence et al. (2018); Martinez Schramm & Hannemann (2019).

As an impulse shock tunnel, the model walls in HEG experiments remain cold with respect to the flow field conditions, with wall-to-recovery temperature ratios in the order of 0.1. Aiming at expanding the achievable temperature ratios, electric heating elements have been used internally in HEG models (Wagner, Martinez Schramm, et al., 2016). Resulting wall temperatures of up to 800 K were measured using an infrared camera IRCam Equus 327k M, corresponding to a wall-to-recovery temperature ratio of 0.3.

The development of the application of temperature sensitive paints (TSP) to determine wall heat flux

in HEG resulted in an applicable system which can be used for low enthalpies so far and is described in Ozawa et al. (2014). The luminophores 4-Methylumbelliferone, or 4MU (Schramm et al., 2017), and Dichlorotris (1,10-phenanthroline) Ruthenium(II) hydrate 98%, or Ru(phen) (Martinez Schramm et al., 2015) have been studied and proven suitable for application in impulse shock tunnels such as HEG. Particle image velocimetry (PIV) has been applied in HEG at a total specific enthalpy of 3.3 MJ/kg. The measured free stream velocity of 2275 m/s agreed to within 2.3% with the computed value, see Kirmse et al. (2011).

A heterodyne laser absorption spectroscopy approach has been developed in HEG to determine NO and H₂O production during hydrogen combustion (Schramm & Luís, 2021). The technique consists in detecting IR wavelength absorption spectra in a μ -second range. An IRsweep IRis-F1 spectrometer with two quantum cascade lasers (QCLs) in the infrared region ($1730\text{-}1790\text{ cm}^{-1}$) is used to generate stable and repeatable IR frequency combs, comprising approximately 200 comb lines with 0.25 cm^{-1} comb-line spacing. Heterodyne beating signals are obtained by using the optical frequency comb technique and detected with high-bandwidth (1 GHz) AC-coupled HgCdTe Vigo PV-4TE-10.6 detectors. The difference in spectral amplitudes between the beam that has travelled through the probing volume (sample beam) and a reference beam allow the verification of absorption of specific frequencies corresponding to NO or H₂O. The experimental setup is such that the sample beam can be delivered directly inside the HEG test section and sent back to the spectrometer using optical fibers.

Focused Laser Differential Interferometry (FLDI) has also been recently introduced at HEG. Interferometric separation distances between 70 and 250 μm are achievable using a Sanderson prism (G. P. Camillo & Wagner, 2022). The setup employs a 200 mW Oxxius LCX-532S DPSS laser source to produce either a 2-by-2 or 1-by-6 array of multi-foci FLDI probes. The latter is achieved by means of a diffraction optical element, with resulting distance of approximately 2 mm between each adjacent probe. The FLDI measurements are detected using Thorlabs DET36A2 photodetectors, combined with SRS SR445A DC-350 MHz preamplifiers at 25x amplification. The experimentally observed frequency bandwidth of the FLDI in HEG is between 160 kHz and approximately 10 MHz (G. Camillo et al., 2023). The lower frequency bound is determined by the sensitivity of the instrument to the nozzle shear layer surrounding the core flow, while the upper bound is limited by the interferometric separation distance, as well as signal-to-noise ratio. The signals are recorded on an AMOtronics transient recorder with DC coupling and up to 100 MHz sampling rate. A computational FLDI script has also been implemented and validated using blast wave measurements (G. Camillo & Wagner, 2023), which allows for direct numerical and experimental comparisons of complex flow fields (G. Camillo et al., 2023).

8 Overview of Research Topics at HEG

The application of the aforementioned diagnostics has permitted aerothermodynamic investigations into multiple flow phenomena, fundamental geometrical configurations as well as flight vehicle scaled models at the HEG. Each of these is elaborated briefly below, with the reader being referred to the citations therein for further reading. Attention is given first to fundamental investigations, leading towards more applied cases and projects undertaken in recent times, and followed by a brief outlook to the activities for which the HEG is particularly well-suited.

Boundary layer transition has been an important topic for hypersonics in general resulting in multiple research efforts in fundamental and applied cases. The accurate prediction of transition location on a hypersonic vehicle could lead to significant savings on thermal protection systems, increased payloads and vehicle fuel efficiency (Karl & Bykerk, 2024). The experimental investigation of boundary layer transition in high enthalpy shock tunnels is therefore important to achieve this goal, due to their simulation of flight-relevant conditions and the possibility for cold-wall experimental test cases.

In hypersonics, second-modes (acoustic modes) are the dominant boundary layer instability. This was also observed in experiments undertaken at the HEG (Laurence et al., 2016) and served as a starting point for further investigations into boundary layer transition and control. The use of temperature sensitive paints (TSP, see above) was also necessary to understand heat flux fields in the transitional



region (Ozawa et al., 2014; Surujhlal & Wagner, 2023) and led to a joint experimental and direct numerical simulation (DNS) investigation of secondary instability breakdown at flight-relevant enthalpies (Hader & Fasel, 2021; Surujhlal & Wagner, 2024).

The control of boundary layer instabilities has also received significant attention, given the possibility of passively dampening acoustic second-mode (Fedorov et al., 2001, 2003). Development of a Carbon-Carbon (C/C)-based material was undertaken and experimentally tested at HEG (Wagner, 2014) followed by the development of a temperature-stable C/C-SiC material (Wagner et al., 2014; Wartemann et al., 2012, 2023), which has the additional property of bearing mechanical and thermal loads (Wagner et al., 2015; Weihs et al., 2008). The use of this material for passive boundary layer control and effusion applications under flight-representative enthalpies was successfully demonstrated in the HEG (G. Camillo et al., 2020; Wagner et al., 2013).

The dominant compressibility effects in high-Mach number flows results in significant stretching of the transitional region (Hader & Fasel, 2021; Koevary et al., 2010). The realisation of well-developed turbulence is often not feasible for realistic model lengths under shock-tunnel testing environments (Hopkins et al., 2021). Forced tripping of the boundary layer is therefore an important consideration for tests concerning turbulent boundary layers carried out in shock tunnel environments. Roughness-induced transition studies were undertaken at the HEG to demonstrate effective tripping of a hypersonic boundary layer to turbulence (Surujhlal et al., 2023). Interspersed roughness elements with a reduced size were shown to successively trip the boundary layer far upstream of natural transition.

The investigation of turbulent boundary layers was carried out by using FLDI in conjunction with LES calculations (G. Camillo et al., 2023). The results obtained by means of FLDI and computational FLDI (cFLDI) demonstrated favourable comparison with the LES for a frequency range between 160 kHz and 1 MHz. This assists further understanding of turbulence under the unique conditions of hypervelocity free streams and cold wall conditions.

A sound knowledge of incoming boundary layer conditions is specifically useful for shock-wave/boundary layer interaction (SWBLI) studies. In these flows, the interaction region is particularly sensitive to the conditions of the incoming boundary layer (Babinsky & Harvey, 2011). Impinging SWBLIs were studied at the HEG using an incoming transitional boundary layer (Wagner, Schramm, & Hannemann, 2016) and an incoming turbulent boundary layer (Wagner & Surujhlal, 2022). Further attention was given to the use of a heated impingement surface heated to over 700 K in order to test at larger wall-to-freestream temperature ratios which are more representative of flight conditions (Volpiani et al., 2019). Furthermore, in the context of the STORT project (Gülhan et al., 2021), ground testing was performed at the HEG in a coupled numerical and experimental study of the surface heat flux in the vicinity of a control surface canard resulting in a SWBLI along the forebody (Ecker et al., 2020, 2023). Various incoming boundary layer states were investigated.

The investigation of scaled flight models has a long history for the HEG. In recent times, the HEXAFLY-INT geometry was extensively investigated using temperature-sensitive paint (TSP) on the windward side of a 1:2.6 scale model for boundary layer transition studies. A coupled numerical and experimental investigation (Wagner et al., 2019) revealed the presence of a vortex pair which was not predicted by the RANS-CFD, illustrating the importance of ground-testing in HEG for such projects. Additionally, the Reusability Flight Experiment (ReFEx) was tested as a 1:4 scaled model with the use of TSP on the forebody and canard. This revealed the presence of a shock-shock interaction at the canard leading edge, which resulted in large surface heat fluxes downstream along the canard surface. Laminar and RANS CFD calculations under- and over-predicted these surface heat fluxes, most probably due to uncertainties in the boundary layer state.

Extensive scramjet combustion studies have been conducted at HEG (Karl et al., 2020). Furthermore, the application of fast-response TSP within the combustion chamber (Schramm & Schmidt, 2021) permitted insights into transient scramjet combustion flows in terms of surface heat fluxes during the hydrogen combustion process. Lastly, heterodyne laser absorption spectroscopy (Schramm & Luís, 2021) was successfully used to identify the mass fractions of combustion components NO and H₂O in a scramjet.

With an outlook to the future, a number of new research topics are pursued at HEG, in particular with emphasis on high-enthalpy hypersonic flows. For instance, the interaction of electromagnetic waves, in a range typically used for radar applications, with plasma formed around hypersonic vehicles at high velocities is currently studied experimentally and numerically (Petervari et al., 2022, 2023). The research objective is also relevant for communication black-out effects during planetary entry (Luis et al., 2024; Luís et al., 2023). Another relevant topic is the experimental quantification of the radiation heat flux in UV-VIS to MWIR bands and its observed over-estimation in shock tunnel measurements (Cruden et al., 2021; Surujhlal et al., 2022; Tanno et al., 2015). This is necessary to systematically reduce uncertainties in future radiation dominated surface heat flux measurements in high-enthalpy ground test facilities.

In conclusion, the range of topics available to research at the HEG has been increasing in scope in recent years. A range of fundamental and applied topics have been demonstrated to be well-suited for investigation in the HEG.

Acknowledgment

All presented achievements are based on a strong HEG-team effort. Therefore, the authors wish to acknowledge the persistent technical support provided by Mr. Schwendtke, Mr. Frenzel, Mr. Glasewald and Mr. Ammer as well as the numerical support provided by Dr. Karl and Dr. Ecker.

References

- Babinsky, H., & Harvey, J. K. (Eds.). (2011). *Shock wave/boundary-layer interactions*. Cambridge University Press.
- Boehrk, H., Wartemann, V., Eggers, T., Martinez Schramm, J., Wagner, A., & Hannemann, K. (2012, September). Shock tube testing of the transpiration-cooled heat shield experiment AKTiV. In *18th AIAA/3AF international space planes and hypersonic systems and technologies conference*. American Institute of Aeronautics and Astronautics. <http://dx.doi.org/10.2514/6.2012-5935>
- Camillo, G., & Wagner, A. (2023, April). Focused laser differential interferometry post-processing methodology for flowfields with circular symmetry. *Review of Scientific Instruments*, 94(4). <http://dx.doi.org/10.1063/5.0132874>
- Camillo, G., Wagner, A., Dittert, C., Benjamin, L., Wartemann, V., Neumann, J., & Hink, R. (2020). Experimental investigation of the effect of transpiration cooling on second mode instabilities in a hypersonic boundary layer. *Experiments in Fluids*, 61, 162. <http://dx.doi.org/https://doi.org/10.1007/s00348-020-02994-8>
- Camillo, G., Wagner, A., Toki, T., & Scalo, C. (2023). Combined experimental and numerical investigation of a hypersonic turbulent boundary layer by means of FLDI and large-eddy simulations. *Aerospace*, 10(6), 570. <http://dx.doi.org/10.3390/aerospace10060570>
- Camillo, G. P., & Wagner, A. (2022, February). A low-effort and inexpensive methodology to determine beam separation distance of multi-foci FLDI. *Experiments in Fluids*, 63(53). <http://dx.doi.org/10.1007/s00348-022-03401-0>
- Cruden, B. A., Tang, C. Y., Olejniczak, J., Amar, A. J., & Tanno, H. (2021, June). Characterization of radiative heating anomaly in high enthalpy shock tunnels. *Experiments in Fluids*, 62(7). <http://dx.doi.org/10.1007/s00348-021-03227-2>
- Ecker, T., Schramm, J., Schmidt, L., Surujhlal, D., & Wagner, A. (2020). Shockwave boundary layer interaction of laminar/transitional flow past a sharp fin. In *HiSST: 2nd international conference on high-speed vehicle science & technology*.



- Ecker, T., Schramm, J., Schmidt, L., Surujhlah, D., Wagner, A., & Horchler, T. (2023). Numerical and experimental investigation of the shockwave boundary layer interaction of laminar/transitional flow past a sharp fin. In *Proceedings of the Aerospace Europe Conference - EUCASS - CEAS - 2023*. CEAS. <http://dx.doi.org/10.13009/EUCASS2023-699>
- Fedorov, A. V., Malmuth, N. D., Rasheed, A., & Hornung, H. G. (2001, April). Stabilization of hypersonic boundary layers by porous coatings. *AIAA Journal*, 39(4), 605-610.
- Fedorov, A. V., Shipliyuk, A., Maslov, A., Burov, E., & Malmuth, N. (2003). Stabilization of a hypersonic boundary layer using an ultrasonically absorptive coating. *Journal of Fluid Mechanics*, 479, 99-124. <http://dx.doi.org/10.1017/S0022112002003440>
- Friedl, D., Martinez Schramm, J., & Hannemann, K. (2016). Measurement of aerodynamic coefficients of blunt cones at the High Enthalpy Shock Tunnel Göttingen. In *11th international workshop on shock tube technology*.
- Gülhan, A., Willems, S., & Neeb, D. (2021, November). Shock interaction induced heat flux augmentation in hypersonic flows. *Experiments in Fluids*, 62(12). <http://dx.doi.org/10.1007/s00348-021-03336-y>
- Hader, C., & Fasel, H. F. (2021). Direct numerical simulations of hypersonic boundary-layer transition for a straight cone at Mach 7. In *AIAA aviation forum*. <http://dx.doi.org/10.2514/6.2021-2865>
- Hannemann, K. (2003, January). High enthalpy flows in the HEG shock tunnel: Experiment and numerical rebuilding (invited). In *41st aerospace sciences meeting and exhibit*. American Institute of Aeronautics and Astronautics. <http://dx.doi.org/10.2514/6.2003-978>
- Hopkins, K. J., Porat, H., McIntyre, T. J., Wheatley, V., & Veeraragavan, A. (2021). Measurements and analysis of hypersonic tripped boundary layer turbulence. *Experiments in Fluids*, 62(8). <http://dx.doi.org/10.1007/s00348-021-03254-z>
- Karl, S., & Bykerk, T. (2024). Sustainable space technologies—strategies toward a predictive aerothermal design of re-useable space transportation systems. *Review of Scientific Instruments*, 95(2). <http://dx.doi.org/10.1063/5.0177075>
- Karl, S., Hannemann, K., Mack, A., & Steelant, J. (2008). Cfd analysis of the hyshot II scramjet experiments in the HEG shock tunnel. In *15th AIAA international space planes and hypersonic systems and technologies conference*. American Institute of Aeronautics and Astronautics. <http://dx.doi.org/10.2514/6.2008-2548>
- Karl, S., Martinez Schramm, J., & Hannemann, K. (2005). Experimental and numerical investigation of high enthalpy flow past a cylinder in heg. In *Shock waves* (pp. 179–184). Springer Berlin Heidelberg. http://dx.doi.org/10.1007/978-3-540-27009-6_24
- Karl, S., Martinez Schramm, J., & Hannemann, K. (2020, March). Post-test analysis of the lapcat-ii subscale scramjet. *CEAS Space Journal*, 12(3), 385–395. <http://dx.doi.org/10.1007/s12567-020-00307-7>
- Karl, S., & Steelant, J. (2018, March). Crossflow phenomena in streamline-traced hypersonic intakes. *Journal of Propulsion and Power*, 34(2), 449–459. <http://dx.doi.org/10.2514/1.b36637>
- Kirmse, T., Agocs, J., Schröder, A., Martinez Schramm, J., Karl, S., & Hannemann, K. (2011, April). Application of particle image velocimetry and the background-oriented schlieren technique in the high-enthalpy shock tunnel göttingen. *Shock Waves*, 21(3), 233–241. <http://dx.doi.org/10.1007/s00193-011-0314-2>

- Koevary, C., Laible, A., Mayer, C., & Fasel, H. (2010, June and July). Numerical simulations of controlled transition for a sharp circular cone at Mach 8. In *40th fluid dynamics conference and exhibit*. Chicago, Illinois: AIAA. (AIAA 2010-4598 Copyright ©)
- Laurence, S. J., Butler, C. S., Martinez Schramm, J., & Hannemann, K. (2018, March). Force and moment measurements on a free-flying capsule in a shock tunnel. *Journal of Spacecraft and Rockets*, 55(2), 403–414. <http://dx.doi.org/10.2514/1.a33820>
- Laurence, S. J., Wagner, A., & Hannemann, K. (2014, July). Schlieren-based techniques for investigating instability development and transition in a hypersonic boundary layer. *Experiments in Fluids*, 55(8). <http://dx.doi.org/10.1007/s00348-014-1782-9>
- Laurence, S. J., Wagner, A., & Hannemann, K. (2016, 6). Experimental study of second-mode instability growth and breakdown in a hypersonic boundary layer using high-speed schlieren visualization. *Journal of Fluid Mechanics*, 797, 471–503. <http://dx.doi.org/10.1017/jfm.2016.280>
- Lu, F. K., & Marren, D. E. (Eds.). (2002). *Advanced hypersonic test facilities* (No. 198). Reston, Va.: American Inst. of Aeronautics and Astronautics. (Includes bibliographical references and index)
- Luis, D., Viladegut, A., Chazot, O., & Camps, A. (2024). Radio frequency signal propagation through a stagnant flow in a plasma facility for analysis of the communication blackout phenomenon. In *AIAA SCITECH 2024 Forum*. American Institute of Aeronautics and Astronautics. <http://dx.doi.org/10.2514/6.2024-1421>
- Lukasiewicz, J. (1973). *Experimental methods of hypersonics* (No. vol. 3). New York, NY: M. Dekker.
- Luis, D., Giangaspero, V., Viladegut, A., Lani, A., Camps, A., & Chazot, O. (2023, November). Effect of electron number densities on the radio signal propagation in an inductively coupled plasma facility. *Acta Astronautica*, 212, 408–423. <http://dx.doi.org/10.1016/j.actaastro.2023.07.028>
- Martinez Schramm, J., & Hannemann, K. (2019). Scramjet thrust measurements an a shock tunnel using completely free-flight and a restrained force measurement set-up. In *International society for air breathing engines congference, canberra, australia*.
- Martinez Schramm, J., Hannemann, K., Ozawa, H., Beck, W., & Klein, C. (2015, March). Development of temperature sensitive paints in the High Enthalpy Shock Tunnel Göttingen, HEG. In *8th European Symposium on Aerothermodynamics for Space Vehicles*.
- Martinez Schramm, J., Karl, S., Hannemann, K., & Steelant, J. (2008, April). Ground testing of the HyShot II scramjet configuration in HEG. In *15th AIAA International Space Planes and Hypersonic Systems and Technologies Conference*. American Institute of Aeronautics and Astronautics. <http://dx.doi.org/10.2514/6.2008-2547>
- Martinez Schramm, J., Wagner, A., Wolfram, J., Hannemann, K., Barth, T., Mulot, J. D., & Schröder, A. (2009, October). Post flight analysis of shefex i: Shock tunnel testing and related cfd analysis. In *16th aiaa/dlr/dglr international space planes and hypersonic systems and technologies conference*. American Institute of Aeronautics and Astronautics. <http://dx.doi.org/10.2514/6.2009-7216>
- Ozawa, H., Laurence, S. J., Schramm, J. M., Wagner, A., & Hannemann, K. (2014, December). Fast-response temperature-sensitive-paint measurements on a hypersonic transition cone. *Experiments in Fluids*, 56(1). <http://dx.doi.org/10.1007/s00348-014-1853-y>
- Petervari, R., Nekris, A., & Bieker, T. (2022, April). Numerical analysis of radar-plasma-signatures of a sphere in a Mach 10 hypersonic wind tunnel flow. In *2021 18th European Radar Conference (EuRAD)*. IEEE. <http://dx.doi.org/10.23919/eurad50154.2022.9784578>



- Petervari, R., Weidner, S., Nekris, A., Brüggewirth, S., & Knott, P. (2023, December). The measurement of radar-plasma signatures in a hypersonic shock tunnel: Simulation and experiment. *IEEE Transactions on Aerospace and Electronic Systems*, 59(6), 8581–8597. <http://dx.doi.org/10.1109/taes.2023.3310497>
- Robinson, M., & Hannemann, K. (2006, June). Short duration force measurements in impulse facilities. In *25th AIAA Aerodynamic Measurement Technology and Ground Testing Conference*. American Institute of Aeronautics and Astronautics. <http://dx.doi.org/10.2514/6.2006-3439>
- Sandham, N., Schüle, E., Wagner, A., Willems, S., & Steelant, J. (2014, July). Transitional shock-wave/boundary-layer interactions in hypersonic flow. *Journal of Fluid Mechanics*, 752, 349–382. <http://dx.doi.org/10.1017/jfm.2014.333>
- Schramm, J. M., Edzards, F., & Hannemann, K. (2017, October). Calibration of fast-response temperature sensitive paints for their application in hypersonic high enthalpy flows. In *New Results in Numerical and Experimental Fluid Mechanics XI* (pp. 141–151). Springer International Publishing. http://dx.doi.org/10.1007/978-3-319-64519-3_13
- Schramm, J. M., & Luís, D. (2021). Experimental approach on concentration measurements of NO in hydrogen combustion based on heterodyne laser absorption spectroscopy using quantum cascade lasers. In *New Results in Numerical and Experimental Fluid Mechanics XIII* (pp. 110–120). Springer International Publishing. http://dx.doi.org/10.1007/978-3-030-79561-0_11
- Schramm, J. M., & Schmidt, L. (2021). Internal application of ultra-fast temperature sensitive paint to hydrogen combustion flow. In *New Results in Numerical and Experimental Fluid Mechanics XIII* (pp. 121–131). Springer International Publishing. http://dx.doi.org/10.1007/978-3-030-79561-0_12
- Stalker, R. J. (1967, December). A study of the free-piston shock tunnel. *AIAA Journal*, 5(12), 2160–2165. <http://dx.doi.org/10.2514/3.4402>
- Surujhlal, D., Pelmoine, M., Wagner, A., & Schramm, J. M. (2022). Fast-response measurements of shock-layer radiation in the High Enthalpy Shock Tunnel Göttingen (HEG).. (Presented at the 9th International Workshop for Radiation of High Temperature Gases for Space Missions)
- Surujhlal, D., & Wagner, A. (2023, October). Fundamental breakdown of second modes in the High Enthalpy Shock Tunnel Göttingen. In *HyFAR-ARA transition symposium book of abstracts*. Bordeaux. (Presented at the 2nd European Symposium on Laminar/Turbulent Transition in the Hypersonic Regime)
- Surujhlal, D., & Wagner, A. (2024). Breakdown of secondary instabilities on a straight cone in a hypersonic shock tunnel. *submitted - under consideration for publication in J. Fluid Mech.*
- Surujhlal, D., Wagner, A., Camillo, G. P., & Martinez Schramm, J. (2023, February). Hypersonic boundary-layer transition on cold-wall canonical geometries with quantified distributed roughness elements. *AIAA Journal*, 61(2), 543–554. <http://dx.doi.org/10.2514/1.j062131>
- Tanno, H., Komuro, T., Lillard, R. P., & Olejniczak, J. (2015, October). Experimental study of high-enthalpy heat flux augmentation in shock tunnels. *Journal of Thermophysics and Heat Transfer*, 29(4), 858–862. <http://dx.doi.org/10.2514/1.t4478>
- Tropea, C., Yarin, A. L., & Foss, J. F. (Eds.). (2016). *Springer Handbook of Experimental Fluid Mechanics*. Heidelberg: Springer.
- Volpiani, P. S., Wagner, A., Bernardini, M., & Larsson, J. (2019, Jan). Using large-eddy simulations to design a new hypersonic shock/boundary-layer interaction experiment. In *AIAA Scitech 2019 Forum*. American Institute of Aeronautics and Astronautics. <http://dx.doi.org/10.2514/6.2019-0098>

- Wagner, A. (2014). *Passive hypersonic boundary layer transition control using ultrasonically absorptive carbon-carbon ceramic with random microstructure* (Doctoral dissertation, Katholieke Universiteit Leuven). Retrieved from <https://lirias.kuleuven.be/handle/123456789/463042>
- Wagner, A., Hannemann, K., & Kuhn, M. (2014). Ultrasonic absorption characteristics of porous carbon-carbon ceramics with random microstructure for passive hypersonic boundary layer transition control. *Experiments in Fluids*, 55(6). <http://dx.doi.org/10.1007/s00348-014-1750-4>
- Wagner, A., Kuhn, M., Martinez Schramm, J., & Hannemann, K. (2013, October). Experiments on passive hypersonic boundary layer control using ultrasonically absorptive carbon-carbon material with random microstructure. *Experiments in Fluids*, 54(10). <http://dx.doi.org/10.1007/s00348-013-1606-3>
- Wagner, A., Martinez Schramm, J., Hickey, J. P., & Hannemann, K. (2016). Hypersonic shock wave boundary layer interaction studies on a flat plate at elevated surface temperature. In *22nd International Shock Interaction Symposium*.
- Wagner, A., Schramm, J., Wartemann, V., Camillo, G., Ozawa, H., & Steelant, J. (2019). Boundary layer transition studies on the HEXAFly-INT hypersonic glide vehicle. In *International Conference on Flight Vehicles, Aerothermodynamics and Re-entry Missions and Engineering (FAR)*.
- Wagner, A., Schramm, J. M., & Hannemann, K. (2016). Experimental hypersonic shock wave boundary layer interaction studies on a flat plate at elevated surface temperature. In *22nd International Shock Interaction Symposium (July, 2016)*. Glasgow.
- Wagner, A., Schülein, E., Petervari, R., Hannemann, K., Ali, S. R. C., Cerminara, A., & Sandham, N. D. (2018, March). Combined free-stream disturbance measurements and receptivity studies in hypersonic wind tunnels by means of a slender wedge probe and direct numerical simulation. *Journal of Fluid Mechanics*, 842, 495–531. <http://dx.doi.org/10.1017/jfm.2018.132>
- Wagner, A., & Surujhlal, D. (2022). *Experimental hypersonic shock/boundary-layer interaction studies on a flat plate at elevated surface temperature* (Tech. Rep.). Arlington, VA: Air Force Office of Scientific Research. (Report ID: AFRL-AFOSR-UK-TR-2022-0026)
- Wagner, A., Wartemann, V., Hannemann, K., Kuhn, M., & Dittert, C. (2015). The potential of ultrasonically absorptive TPS materials for hypersonic vehicles. In *20th AIAA International Space Planes and Hypersonic Systems and Technologies Conference*.
- Wartemann, V., Luedeke, H., & Sandham, N. D. (2012, June). Numerical investigation of hypersonic boundary-layer stabilization by porous surfaces. *AIAA Journal*, 50(6), 1281-1289. <http://dx.doi.org/10.2514/1.J051355>
- Wartemann, V., Wagner, A., Surujhlal, D., & Dittert, C. (2023, June). OCTRA as ultrasonically absorptive thermal protection material for hypersonic transition suppression. *CEAS Space Journal*, 15(6), 959–969. <http://dx.doi.org/10.1007/s12567-023-00504-0>
- Weihs, H., Longo, J., & Turner, J. (2008). Key experiments within the SHEFEX II mission. In *International Astronautical Conference 2008*. Glasgow, Scotland UK.